SSRG International Journal of Applied Physics
ISSN: 2350-0301/ https://doi.org/10.14445/23500301/IJAP-V12I1P101

Volume 12 Issue 1, 1-11, Jan-Apr 2025

Original Article

Performance Investigation of Digital Optical Phase Conjugation-based Optical Switch

Havyarimana Claver[1*], Maniragarura Nestor[2]

[1,2]*Department of Physics, University of Burundi, Bujumbura, Burundi.*

[*]*Corresponding Author : claver.havyarimana@ub.edu.bi*

Received: 06 February 2025 Revised: 19 March 2025 Accepted: 11 April 2025 Published: 25 April 2025

Abstract *- The performance of an optical switch based on Digital Optical Phase Conjugation (DOPC) is investigated. By numerical simulations using the Finite Difference Time Domain (FDTD) method, the operation of the optical switch is demonstrated, and Insertion Loss (IL) and Crosstalk (CT) are evaluated over a range of wavelengths for both Transverse Electric (TE) and Transverse Magnetic (TM) polarizations. The switch is designed utilizing the DOPC technique and incorporates a Multimode Interferometer (MMI) coupler and Distributed Bragg Gratings (DBG) mirrors/filters. Simulation results reveal that these switches exhibit wide bandwidth, low polarization-dependent loss, and compact size. The minimum insertion loss and crosstalk for a single-wavelength switch are 0.45 dB at 1560 nm and -17.5 dB, respectively. For a forward DOPC switch, these values are 0.64 dB and -16.5 dB at 1550 nm. The switch is wavelength selective, with performance limited by the selectivity of the DBG filter, which must have a narrow bandwidth of 0.8 nm for the Dense Wavelength Division Multiplexing system.*

Keywords *- Optical switch, Digital Optical Phase Conjugation, Finite difference time domain.*

1. Introduction

Due to the invention of low-loss optical fibers [1], optical amplifiers [2], and Dense Wavelength Division Multiplexing (DWDM) technologies [3], the transmission capacity of optical communication systems has reached unprecedented levels [4]. However, this progress has shifted the primary bottleneck from the transmission medium to the switching functionalities at the network nodes. Traditional switching architectures rely on Optical-to-Electrical-to-Optical (OEO) conversions, introducing latency, increased energy consumption, and limited scalability- particularly problematic in data centers and high-performance computing environments where bandwidth demand continues to grow due to emerging technologies such as Artificial Intelligence (AI), cloud computing, and real-time analytics [5-8]. Optical switching has become a crucial technology to overcome these limitations by enabling signal routing entirely in the optical domain. This eliminates the need for OEO conversions and allows network operations to remain within the optical layer, thereby preserving transmission speed, reducing energy consumption, and supporting protocol transparency. Despite extensive development of various optical switch architectures-including those based on directional couplers, microring resonators, and Mach-Zehnder interferometers-no existing solution fully satisfies the combined requirements of low Insertion Loss (IL), low Crosstalk (CT), large bandwidth, polarization insensitivity, compactness, and scalability [9-11]. Although the concept of an optical switch based on the Digital Optical Phase Conjugation (DOPC) technique [12-15] was introduced in 2013 [16, 17], its performance characteristics have not yet been investigated in detail to establish its suitability in practical systems. While initial studies highlighted its conceptual feasibility and potential advantages- such as polarization independence and wavelength selectivity- a thorough analysis of performance metrics such as Insertion Loss (IL) and Crosstalk (CT) remains lacking in the literature. This article addresses that gap by presenting an in-depth performance study of the DOPC-based optical switch through numerical simulations. The main objective is to comprehensively evaluate this switching architecture, offering valuable insights for system designers and researchers seeking alternatives to conventional integrated optical switches. The study begins by recalling the working principle of the DOPC-based switch, especially for readers unfamiliar with previous works. The analysis then focuses on the computation of insertion losses and crosstalk over a wide range of wavelengths and for both TE and TM polarizations, thereby evaluating the switch's sensitivity to polarization. This information is essential for assessing the practical relevance of the DOPC-based switch and comparing it against other existing architectures [18-23]. The design relies on Distributed Bragg Gratings (DBGs) [24] or Distributed Bragg Reflectors (DBRs) to achieve wavelength-selective reflection. At the same time, phase modulators are employed to direct the reconstructed optical field toward the desired output ports. The switch is integrated with a Multimode Interference (MMI) coupler to decompose and recombine the optical field, enabling compact and stable signal routing [25-27]. This article is structured as follows: Section 2 describes the materials and methods, beginning with the structure and operational principle of a DOPC-based optical switch for a single wavelength, followed by a detailed performance evaluation, including insertion loss and crosstalk analysis. The next subsection examines the design and functionality of a wavelength-selective DOPC-based switch, while a subsequent part introduces the concept and simulation of forward DOPC-based switching. Prior to the conclusion, Section 3 presents a comprehensive discussion of the simulation results, emphasizing key observations, potential enhancements, and the broader implications for integrated photonic switching architectures.

2. Materials and methods

2.1. Single Wavelength DOPC-based Optical Switch

2.1.1. The Switch Structure and Switching Principle

Figure 1 provided a detailed design for demonstration purposes. The DOPC-based switch comprises a 4×4 MMI connected via tapers to 4 single-mode waveguides, phase modulation elements P and DBG reflectors. The length of the designed MMI is L=315.29 µm, and the width is W=12 µm. The cores of all the single-mode waveguides are w_c = 0.64 µm wide. They are separated by d=3 µm. The parameters of the tapers on the left side are l_{t1}=6 µm and w_{t1}=1.5 µm, while on the right side, they are l_{t2}=19 µm and w_{t2}=1.8 µm. The role of a taper is to minimize the loss caused by a bad self-image. On the right side, the taper is longer to get rid of other excited modes. The length of the phase shift element and DBR mirror are l_p=80 µm and l_m=50 µm, respectively. The total height of the cladding is 2×cl=4 µm.

When a light signal is input from the u^{th} waveguide at the left side of an MMI, like in the structure in Figure 1, it creates fields with phases Φ^{u}_{right} at the right side. If the phases Φ^{u}_{right} are set to their conjugation $\overline{\Phi^{u}_{right}}$ by optical phased conjugate reflection with the aid of elements P and DBG, the light signal would return to the u^{th} waveguide due to the reciprocity of an optical path. A light signal inputted from the v^{th} waveguide at the left side might be reflected back following the same principle. To switch the light signal from the u^{th} to the v^{th} port, we need only to add a phase modulation. $\Delta\Phi_{u,v}$ to $\overline{\Phi^{u}_{right}}$ to make it equal $\overline{\Phi^{v}_{right}}$ as indicated by the equation,

$$\overline{\Phi^{v}_{right}} = \overline{\Phi^{u}_{right}} + \Delta\gamma_{u,v} \tag{1}$$

Where $\Delta\gamma_{u,v} = [\bar{\gamma}_{1,v} - \bar{\gamma}_{1,u}, \bar{\gamma}_{2,v} - \bar{\gamma}_{2,u}, \dots, \bar{\gamma}_{n,v} - \bar{\gamma}_{n,u}]$

Under the control of digitally generated voltage, the refraction index of electro-optical material on each waveguide at the right side can be precisely adjusted by an amount of Δn_k such that the condition of Equation (1) is satisfied, which yields.

$$\frac{2\pi}{\lambda_m}\Delta n_k(2l) = \overline{\gamma_{u,k}} - \gamma_{u,k} \tag{2}$$

Where λ_m is the wavelength of the light signal, l the length of the P element, Δn_k the refractive index variation in the k^{th} waveguide due to electro-optic effect, k = 1,2,…, B. The Right Hand Side of Equation (2) expresses the difference between the conjugate phases of the light field from the v^{th} waveguide and the phase of the light field from the u^{th} waveguide in the single mode waveguide k. With the designed switch in Figure 1, the phase in each single-mode waveguide at the right side was calculated using Equation (3) [25]. Phase data are needed to determine how phase modulation will be done for a desired switching. Calculated refractive index shifts, Δn_k were deduced from Equation (2). The calculated phase shifts are for switching light signals from port 4 to ports 1, 2 and 3, respectively. The length of the phase modulation section is set as 80 µm to keep the refraction index change Δn_k needed to produce 2π phase modulation at the order of 10^{-3}

$$\gamma_{u,k} = \begin{cases} \frac{\pi}{4N}(k-u)(2N-k+u)+\pi \\ \quad if\ \ u+k\ \ is\ even \\ \frac{\pi}{4N}(u+k-1)(2N-u-k+1) \\ \quad if\ \ u+k\ \ is\ odd \end{cases} \tag{3}$$

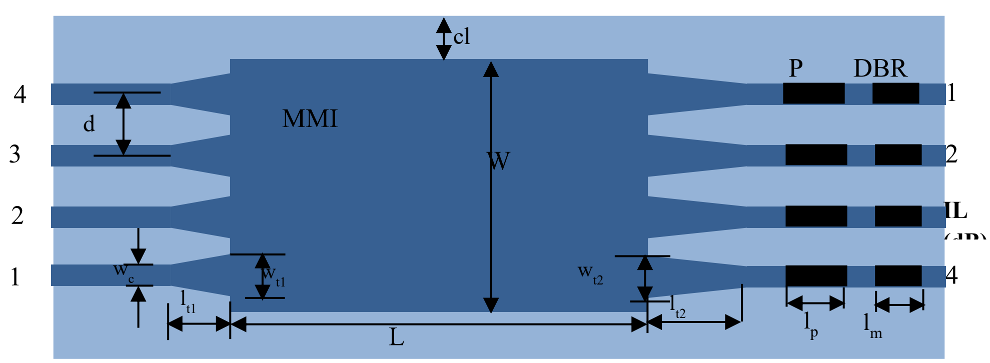

Fig. 1 Structure of a DOPC-based optical switch

2.1.2. Performance Analysis

Before addressing the key performance parameters of optical switches, it is important to emphasize that the chosen switching scheme strongly influences overall performance. In addition to the basic characteristics discussed in the previous section, scalability and fabrication tolerance must also be considered. Scalability refers to the ability of a switching architecture to accommodate an increasing number of ports within an optical path, which is essential for high-capacity routing systems. It is not a single, easily quantifiable parameter but rather a multifaceted property influenced by factors such as insertion loss, extinction ratio, device footprint, power consumption, physical size, and cost. Fabrication tolerances are equally critical during the manufacturing process and under operational conditions.

Geometrical precision during fabrication significantly affects device performance. Previous studies have shown that Multimode Interference (MMI) devices offer high tolerance to fabrication errors [25]. Given this advantage, the DOPC-based optical switch described in this work is designed using an MMI coupler to benefit from its inherent robustness and tolerance. The switch will then benefit the general advantages of MMI devices, including fabrication tolerance. Operation tolerances relate to the device performance when changes in the wavelength, polarization, temperature, input field distribution or refractive index occur. Operation tolerance and control technology are dependent on the material used. In the performance analysis, particular attention is given to the most critical parameters commonly used to evaluate optical switches, Insertion loss is defined as the ratio of light power P_{output} in the desired output waveguide to the light power P_{input} in the input waveguide namely Insertion Loss (IL), Crosstalk (CT), bandwidth, and Polarization-Dependent Loss PDL).

$$I = -10\log\left(\frac{P_{outpout}}{P_{inpout}}\right) = -10log\left(\frac{E^2_{output}}{E^2_{input}}\right) \quad (4)$$

Where E_{output} and E_{input} are field amplitudes in output and input ports, respectively. The CT, which is the ratio of light power $P_{undesired}$ in the undesired waveguide to the light power $P_{desired}$ in the desired waveguide, is expressed in Equation (5).

$$CT = 10\log\left(\frac{P_{indesirée}}{P_{souhaitée}}\right) = 10\log\left(\frac{E^2_{undesired}}{E^2_{desired}}\right) \quad (5)$$

Loss (IL), Crosstalk (CT), bandwidth, and Polarization-Dependent Loss (PDL). where $E_{undesired}$ and $E_{desired}$ are field amplitudes in undesired and desired waveguides, respectively. Figure 2 illustrates Finite Difference Time Domain (FDTD) [28-30] simulations of DOPC-based switching for one working wavelength λ=1550 nm. The right arrow indicates the input direction, and the left arrow indicates the output. The guiding core has 3.39 as its refractive index, while the cladding has 3.17. The size of the switch is 500 μm×16 μm, as it is indicated in the figure. As shown in Figure 2 (a), TE mode light signals inputted in port 4 were switched to port 1. In Figure 2(b), the input light signal was set in TM mode to check polarisation dependence, and it was successfully switched to port 1, the same as in TE mode. Based on simulations in Figure 2, such performances as IL, CT and polarization sensitivity for the device were calculated with Equation (4) and Equation (5) for IL and CT, respectively. In Table 1, the slight difference between the two polarizations in IL and CT indicates that the device has a low polarization dependency. Actually, Polarization-independent operation is possible by designing at an intermediate length at the price of a small loss increase. B. Lucas et al. [25] have discussed these issues for MMI devices, and the conclusion is the same: MMI-based devices have low polarization dependence. IL and CT were calculated for output ports 2 and 3, as illustrated in Figure 2 (c), and TE mode. As values in Table 1 indicate, the IL is less or equal to 1dB. The CT varies between -19 dB to -12 dB for TE mode.

The CT to port 4 needs special treatment because the light field is reflected to the source. So, an antireflection should be used between the switch's source and input port. For more bandwidth checks of the device, one wavelength was set at the lowest possible wavelength of λ_1=1537nm. The condition of a single-mode waveguide determines this wavelength. Below 1537 nm, our waveguides designed for in/output become multimode. Another wavelength was set at the largest possible wavelength of λ_2=1586nm. The MMI coupler was designed for 1550 nm. The length of an MMI is wavelength dependent, so above 1586 nm, the self-images are not formed at the desired length. This results in reflections leading to high IL and CT. Therefore, the device exhibited a bandwidth of 49 nm. With a bandwidth of 49 nm, one switch based on DOPC can handle about 61 wavelengths with a gap of 0.8 nm for DWDM application. The analysis of Insertion Loss (IL) and Crosstalk (CT) for the DOPC-based optical switch, as given in Figures 3 and 4, highlights its robust performance and suitability for optical communication systems. Insertion Loss (IL): The switch exhibits low IL in the operational wavelength range (1540–1570 nm), with values below 2 dB for both TE and TM modes in the central wavelength region (~1550 nm). In addition, the IL increases at the spectral edges, indicating some wavelength dependence, but remains within acceptable limits for practical applications. Finally, the low polarization dependence suggests that the switch maintains efficient signal transmission for different polarization states.

Crosstalk (CT): The switch demonstrates low crosstalk, with values consistently below -10 dB, ensuring minimal signal leakage between ports. TE mode generally exhibits better isolation than TM mode, though the difference remains moderate. Crosstalk slightly increases at longer wavelengths (>1560 nm), which could be attributed to modal dispersion or coupling inefficiencies.

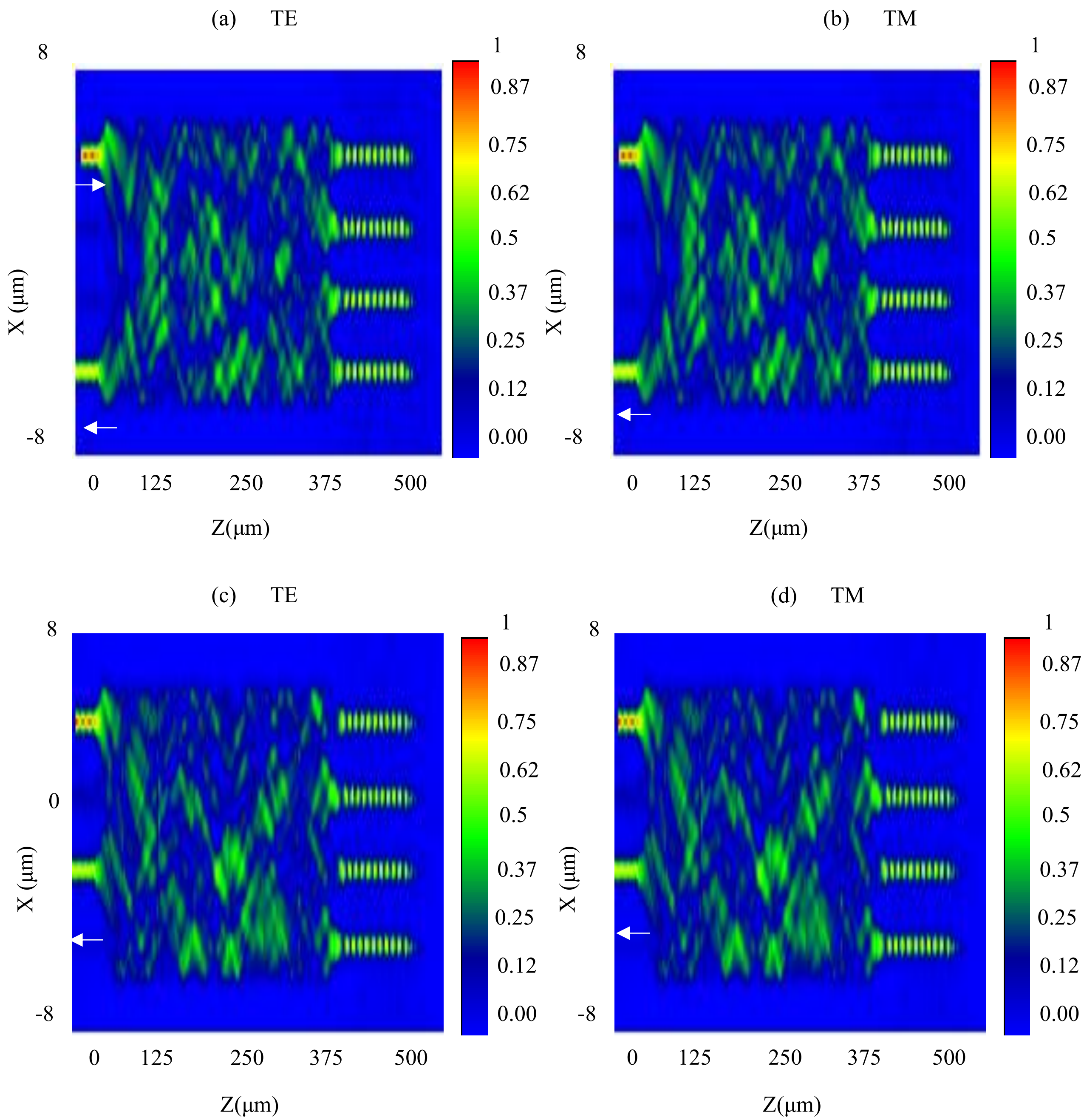

Fig. 2 Switching of one wavelength λ=1550 nm using an optical switch based on DOPC: (a) TE mode from port 4 to 1, (b) TM mode, (c) TE mode from port 4 to 2 and (d) TM mode from port 4 to 2.

Table 1. DOPC OS performance for λ=1550 nm

Switched from input port 4 to port j		IL (dB)	CT(dB)			
			Output port 1	Output port 2	Output port 3	Input port 4
1	(TM)	1.002		-13.560	-13.628	-18.884
	(TE)	0.961		-12.15	-11.92	-15.12
2 (TE)		0.9345	-16.455		-12.497	-16.692
3 (TE)		1.0288	-14.388	-15.820		-16.625

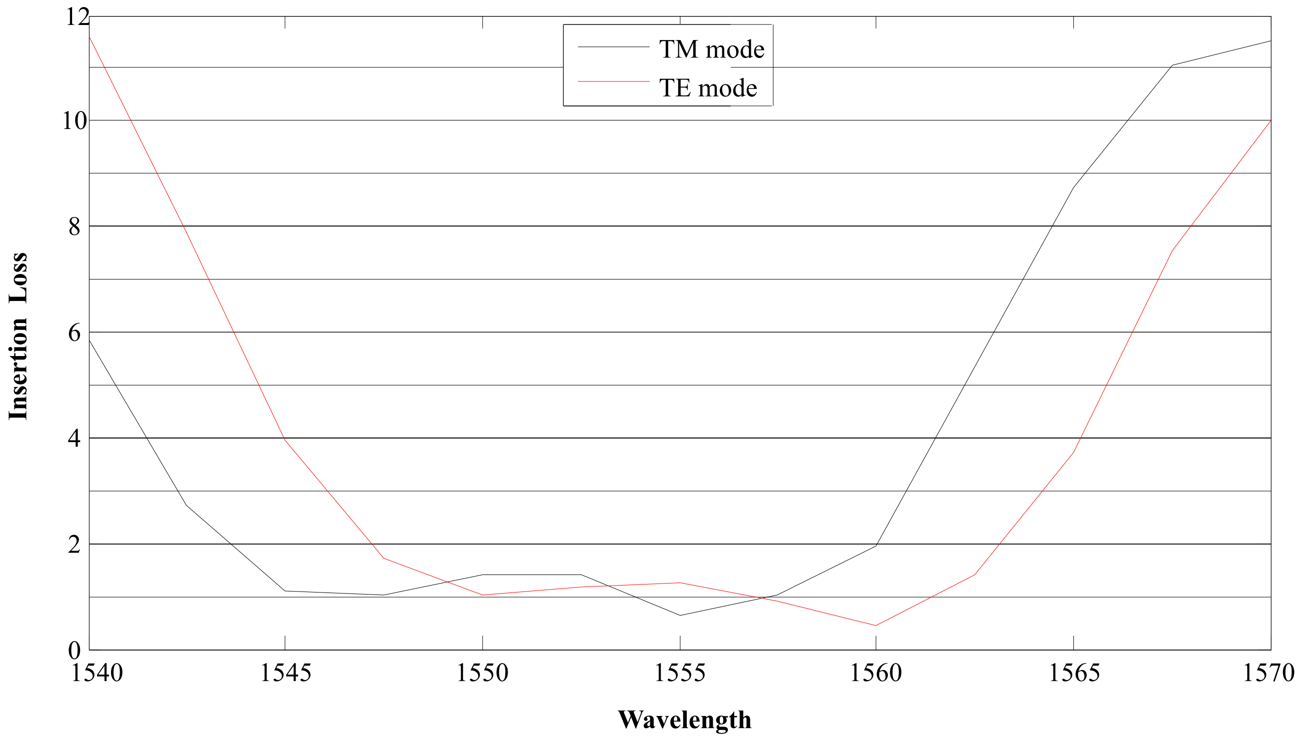

Fig. 3 DOPC-based Optical Switch IL per wavelength for TE and TM modes

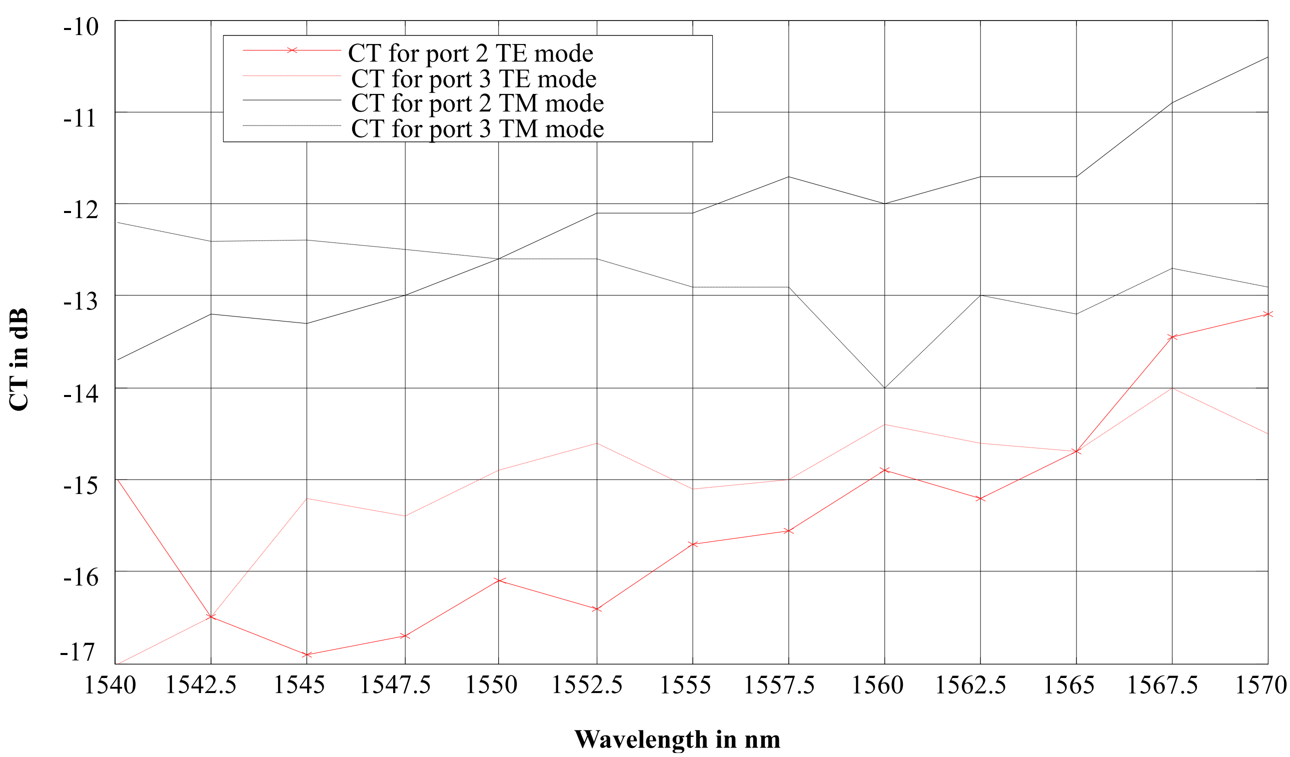

Fig. 4 DOPC-based Optical Switch CT per wavelength for TE and TM modes

2.2. DOPC-based Wavelength Selective Optical Switch

In wavelength-selective DOPC-based optical switching, it is essential to address two key requirements: (1) performing DOPC switching independently for each wavelength and (2) preventing the switching of one wavelength from interfering with the propagation of others. To satisfy the first requirement, the design shown in Figure 5 includes the elements Pm and DBGm, which are responsible for executing DOPC individually for each wavelength λm, following the same principles described in previous subsections. To fulfill the second requirement, a complementary phase modulation element is introduced to eliminate cross-interference between wavelength channels and ensure proper isolation during switching operations CP_m with the same length of P_m for wavelength λ_m. Without $CP_{m,}$ switching one wavelength λm will change the phases of all the unselected wavelengths that pass through DBGm because they will also experience the phase modulation described by Equation (2) for all waveguides k at the right side. As a result, every time wavelength λ_m was switched, the unselected wavelengths that pass through DBG_m would all be affected. However, when CP_m are added, each CP_m can be made to produce a complementary phase modulation Δcn_k so that,

$$\frac{2\pi}{\lambda_m}(\Delta n_k + \Delta cn_k)(2l) = constant \quad (5)$$

Now, all the wavelengths that pass through DBG_m experience firstly a phase shift controlled by Δn_k and then followed by a phase shift controlled by Δcn_k. When Equation (5) is fulfilled, the total phase shift will be the same. In other words, all the wavelengths that pass through DBG_m would behave as if they traveled an extended but identical length on every waveguide at the right side. Therefore, the switching of wavelength λ_m brings little influence to other wavelengths. In a word, independent multi-wavelength switching becomes possible with the help of complementary phase modulation elements. As explained above, for switching of one wavelength λ_m, a phase modulation section P_m, a DBG_m and a complementary phase modulation section CP_m are needed, which are all arranged on the straight waveguides on the right side. This serial arrangement brings two advantages. Firstly, the switch is nonblocking. Secondly, avoiding slow bends results in a compact size. In Figures 6 (a) and 6 (c), FDTD simulations illustrate the simultaneous switching of two wavelengths for TM and TE mode, respectively. The two wavelengths, 1565 nm and 1550 nm, are inputted in port 4 and counted from down to top on the left side at the same time. They are switched to port 1 and port 2, respectively, exerting slight influence on each other owing to the compensation of the complementary phase modulation. Each of the P_m elements and the CP_m has a length of 80 µm. The DBG filter has a length of 50 µm; its Bragg period is 0.2338 µm long.

The DBR mirror for the wavelength 1565 nm has the same length as the filter, and its Bragg period length is 0.2386 µm. To check the influence of P_m and CP_m and the DBR on the performance, the second wavelength was switched alone using the same device, same phase modulation and complementary phase modulation as in Figure 6 (a) and Figure 6 (c) but with another unprocessed wavelength. The simulations are illustrated in Figure 6 (b) and Figure 6 (d) for TM and TE mode, respectively. There is a high CT for TE for port 2. But this CT might come from wavelength λ_1 because it was also reflected back by DBR but with wrong phase modulation. IL and CT are listed in Table 4. IL and crosstalk values in Table 2 show that phase modulation, complementary phase modulation, and DBG filter have an influence on performance. IL increases compared to the single wavelength switch in the previous section. The first and 3rd rows in the same Table show polarization and filter effect, respectively. To identify the effect of the filter, the same device was used with filter and without in the second, respectively. In both cases, phase modulation and complementary phase modulation are maintained. It comes out that the effect is the DBG, which is most influential in the DOPC wavelength selective switch. Parameters in the third row in the table contain noises from the other wavelength. This is the reason why CT is high.

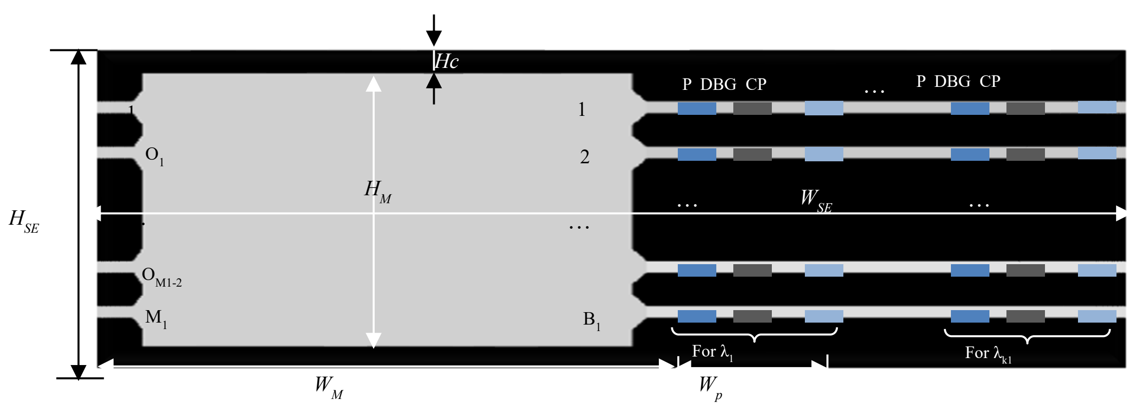

Fig. 5 The structure of a 1×(M-2)×K DOPC-based wavelength selective switch

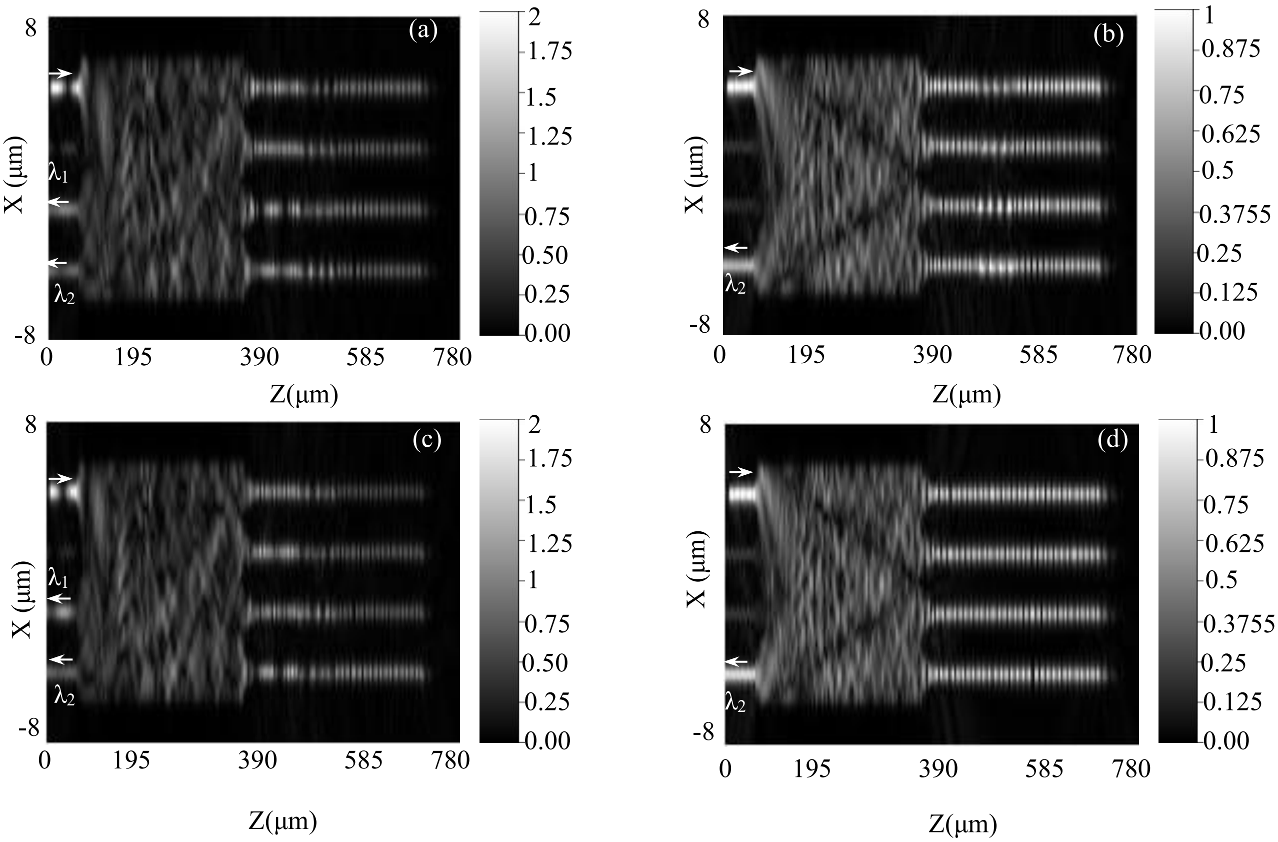

Fig. 6 DOPC-based simultaneous switching of two wavelengths λ_1=1550 nm, λ_2=1565nm TM (a) TE mode, (c) Single wavelength, λ_2, passing through the filter, (b) without filter, and (d) for TM mode.

Table 2. Performance of WSS for wavelength λ_2 =1565 nm

Condition of switching	IL(dB)	CT(dB)		
		Output port 4	Output port 3	Output port 2
With P, CP and filter for λ_1 (TM\ TE)	2.44\2.74	-13.75\-15.13	-10.79\-11.86	-11.62\-4.95
With P, CP and without filter for λ_1 (TM)	0.8766	-15.2331	-11.1646	-10.6585
Simultaneously with λ_1 (TM\ TE)	1.03\1.9	-9.54\-11.69	-6.25\-6.8	-

A DOPC wavelength selective optical switch relies on a DBG filter for wavelength selective reflection. To maintain low IL and low CT, it is highly desired that a DBG reflect only one working wavelength and let all other working wavelengths pass. In a DWDM network, the channel space might be as small as 0.8 nm. So, DBG filters must be designed carefully to provide a narrow stop band. Details for the reflectance spectrum for 1550 nm working Bragg wavelength, DBG filter structure and spectrum for TE mode are provided in our previous work [13].

2.3. Forward DOPC-based Optical Switch

As previously mentioned, DOPC enables field reconstruction in the backward direction, meaning both the input and output waveguides are positioned on the same side of the MMI. However, by introducing an additional MMI, as illustrated in Figure 7, DOPC can also be implemented in the forward direction. This design closely resembles an N×N MMI-Mach Zehnder Interferometer (MZI) switch, a structure that has gained significant interest due to the advantages of MMI technology, particularly for large-port optical switches [8]. The switching function is achieved through phase modulation, similar to the backwards-DOPC switch configuration. The key difference lies in the propagation length L of the phase shift section, which replaces 2L in Equation (2), while the indices u and v are counted in the same order, as shown in Figure 7. Unlike the backward DOPC switch, the forward DOPC configuration does not require Distributed Bragg Gratings (DBGs) for reflection or a Complementary Phase (CP) modulation mechanism. Consequently, this approach is limited to switching only a single wavelength at a time. The principle of DOPC in the forward direction has been demonstrated in previous work [12]. By directing the optical signal from a given input port to another port of the same number and applying appropriate phase modulation, the signal can be redirected to a desired output port. In this way, the switching function is successfully achieved.

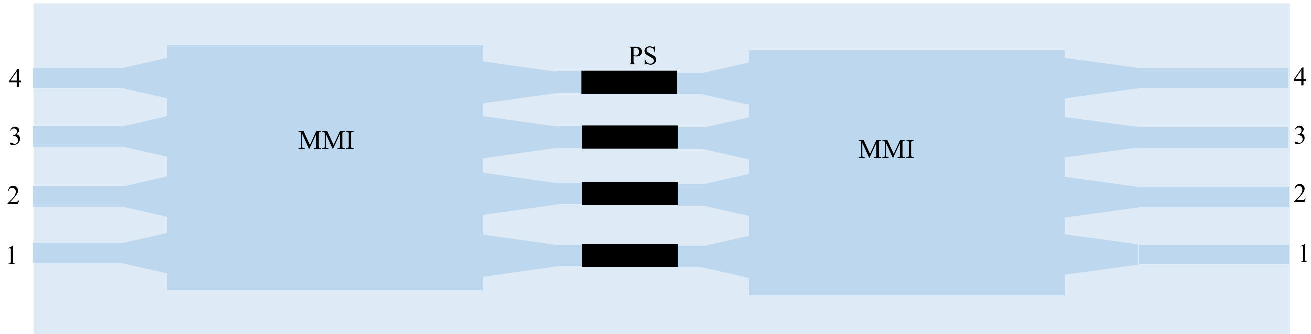

Fig. 7 Forward DOPC-based OS structure

Table 3. Forward DOPC-based optical switch IL and CT for TM mode and wavelength λ=1550 nm

Switched from input port 4 to port j	IL (dB)	CT(dB)			
		Output port 1	Output port 2	Output port 3	Output port 4
1	0.7716	-	-11.9003	-12.30	-15.08
2	0.7526	-16.94	-	-11.74	-12.73
3	0.6490	-13.60	-21.25	-	-13.86
4 (TE/TM)	1.11/ 1.44	-10.73/-7.89	-12.97/-10.65	-13.55/-10.97	-

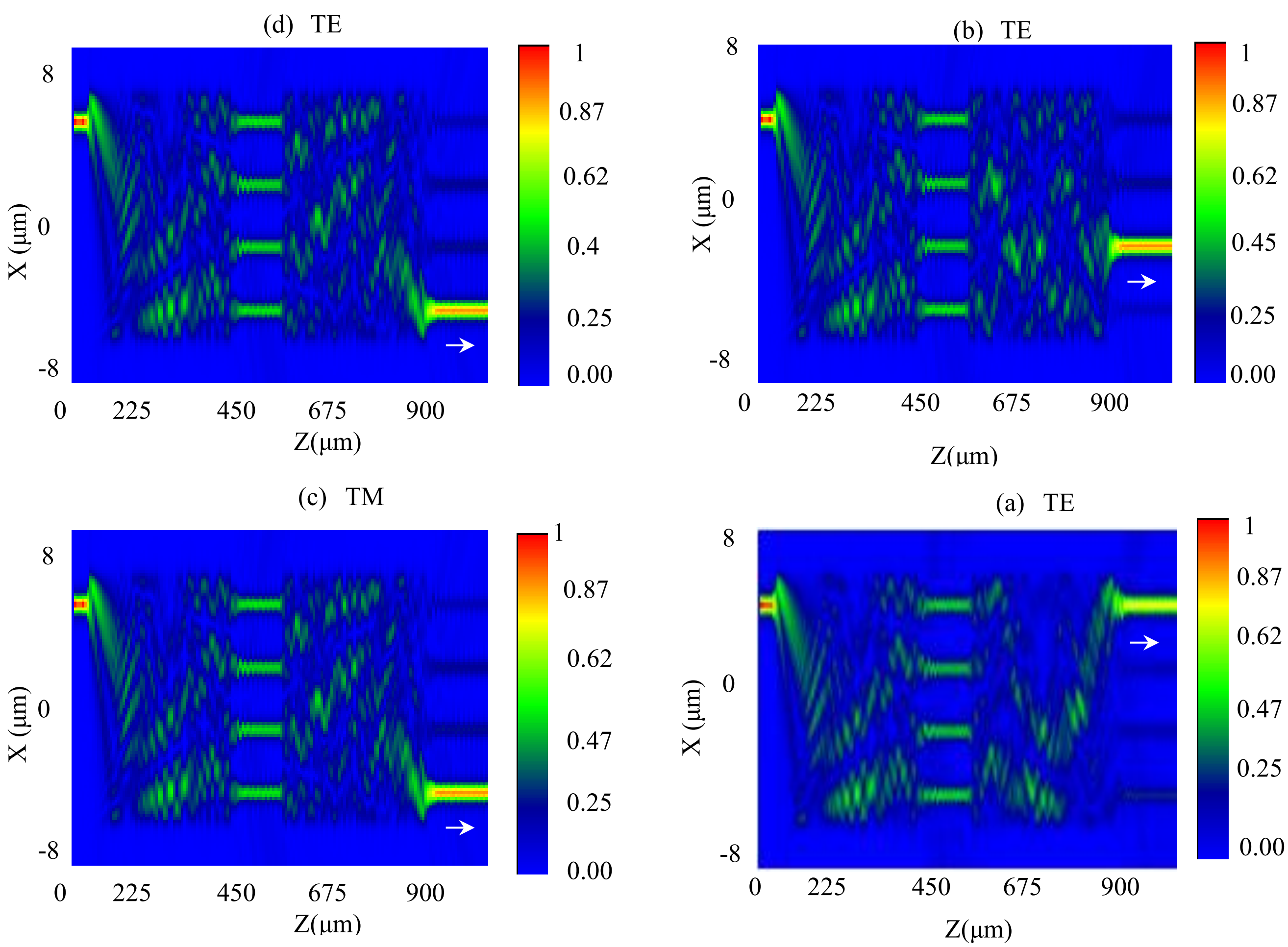

Fig. 8 Forward DOPC-based OS switching for λ=1550 nm from port 4 to port 1 (a) TE mode, 2 (b) TM mode, 2 (c) and 4 (d) for TE mode.

Figure 8 illustrates FDTD simulations for the forward DOPC switch from port 4 to ports 1, 2 and 4 for a TE and TM polarized mode of wavelength 1550 nm. The length of the phase shifter is 80 µm. The in/output port order is counted in the same way: down to the top at both the left and right sides of the switch. Inversed order is for the in between waveguides. The arrows indicate the direction of the light signal propagation. The size of the switch is $H_{MZ}\times W_{MZ}$=900 µm×16 µm.The IL, CT and polarization dependence are shown in Table 3. Also, the forward DOPC-based switch exhibits low IL in the operational wavelength range (1550 nm), with values below 1.5 dB for both TE and TM modes. It also demonstrates low crosstalk. Another advantage of this kind of switch is the possibility of having a switch with a large number of ports.

3. Discussion

The simulation results presented in Figures 2 and 8, along with the Insertion Loss (IL) and Crosstalk (CT) values calculated from the simulated data and summarized in Tables 1, 2, and 3, as well as Figures 3 and 4, demonstrate that the proposed Digital Optical Phase Conjugation (DOPC)-based optical switch exhibits promising performance characteristics. With an Insertion Loss (IL) below 1 dB and Crosstalk (CT) levels as low as -17 dB, the switch maintains high signal integrity across a broad wavelength range. These results confirm the low-loss and low-noise operation of the device, which are essential metrics for practical deployment in optical networks. One of the key advantages of this switch lies in its integration into a photonic circuit, offering compactness, improved robustness, and scalability. Unlike free-space optical switches that often suffer from alignment issues, the integrated nature of the DOPC-based design minimizes mechanical instability and environmental sensitivity.

Furthermore, thanks to the incorporation of Distributed Bragg Gratings (DBGs), the switch achieves wavelength selectivity, allowing individual wavelength channels to be routed independently an essential feature for Dense Wavelength Division Multiplexing (DWDM) systems. Compared to many conventional integrated optical switches such as those based on directional couplers or microring resonators which often exhibit polarization sensitivity, wavelength-dependent performance, or losses due to waveguide bends, the DOPC-based switch demonstrates low polarization dependence. This feature is critical for maintaining consistent performance regardless of signal polarization, reducing the need for complex polarization management. To obtain such results, certain design conditions must be carefully met. The Multimode Interference (MMI) coupler must be precisely designed so that output ports coincide with the self-imaging positions of the input field. Additionally, the transition from the MMI region to the single-mode output waveguides should be optimized using tapered structures, which help reduce mode mismatch and minimize insertion loss. Similarly, the DBGs must strictly satisfy the Bragg condition—i.e., the period of the grating must match the desired reflection wavelength according to $\lambda = 2n\Lambda$—to ensure efficient wavelength-selective reflection without introducing excess loss or spectral distortion. Moreover, the DOPC architecture allows multi-wavelength operation by replicating each wavelength's conjugation and filtering structure. This flexibility gives the switch an edge over other fixed or narrowband switching mechanisms.

4. Conclusion

This study investigated the performance of an optical switch based on Digital Optical Phase Conjugation (DOPC). This technique does not use nonlinear materials and enables precise control of optical wavefront reconstruction. By integrating this principle with a Multimode Interference (MMI) coupler and Distributed Bragg Grating (DBG) filters, the switch achieves low insertion loss, minimal crosstalk, and reduced polarization sensitivity, all within a compact integrated structure. The switch demonstrated efficient signal routing across multiple wavelengths through numerical simulations using the Finite Difference Time Domain (FDTD) method, confirming its potential for Dense Wavelength Division Multiplexing (DWDM) applications.

The results highlight that the switch demonstrates reliable and scalable performance with an optimized MMI design, ensuring self-imaging and proper tapering and the accurate DBG design fulfils the Bragg condition. Compared to conventional integrated and free-space switches, the DOPC-based solution offers significant advantages in terms of wavelength selectivity, polarization independence, and integration potential, making it particularly suited for high-capacity, low-latency optical networks, such as those required in AI-driven data centres and on-chip photonic systems. Future work may explore experimental validations and integration with control electronics to fully realize the practical potential of DOPC-based photonic switching platforms.

Acknowledgments

This paper was supported by the research and innovation department of the University of Burundi.

References

[1] Yoshiaki Tamura et al, "Lowest-Ever 0.1419-dB/km Loss Optical Fiber," *Optical Fiber Communication Conference Postdeadline Papers*, OSA Technical Digest, Optica Publishing Group, 2017. [CrossRef] [Google Scholar] [Publisher Link]

[2] Ashish Bhardwaj et al., "An InP-Based Optical Equalizer Monolithically Integrated with a Semiconductor Optical Amplifier," *IEEE Photonics Technology Letters*, vol. 19, no. 19, pp. 1514-1516, 2007. [CrossRef] [Google Scholar] [Publisher Link]

[3] C.A. Brackett, "Dense Wavelength Division Multiplexing Networks: Principles and Applications," *IEEE Journal on Selected Areas in Communications*, vol. 8, no. 6, pp. 948-964,1990. [CrossRef] [Google Scholar] [Publisher Link]

[4] Global Networking Trends Report, Cisco, pp. 1-34, 2024. [Online]. Available: https://www.cisco.com/c/dam/global/en_uk/solutions/enterprise-networks/2024-global-networking-trends.pdf

[5] Govind P. Agrawal, *Fiber-Optic Communications Systems*, John Wiley & Sons, pp. 1-546, 2002. [Google Scholar] [Publisher Link]

[6] Tarek S. El-Bawab, *Optical Switching*, Springer US, pp. 1-451, 2006. [Google Scholar] [Publisher Link]

[7] Ivan P. Kaminow, and Thomas L. Koch, *Optical Fiber Telecommunications IIIA*, Elsevier Science, 1997. [Google Scholar] [Publisher Link]

[8] S. Tibuleac, and M. Filer, "Trends in Next-Generation ROADM Networks," *Proceedings of the 37th European Conference and Exhibition on Optical Communication*, 1-3, 2011. [Google Scholar] [Publisher Link]

[9] Sangyoon Han et al., "Large-Scale Silicon Photonic Switches with Movable Directional Couplers," *Optica*, vol. 2, no. 4, pp. 370-375, 2015. [CrossRef] [Google Scholar] [Publisher Link]

[10] A. Himeno et al., "Silica-Based Low Loss and High Extinction Ratio 8×8 Thermo-Optic Matrix Switch with Path-Independent Loss Arrangement Using Double Mach-Zehnder Interferometer Switching Units," *Proceedings of European Conference on Optical Communication*, Oslo, Norway, vol. 4, pp. 149-152, 1996. [Google Scholar] [Publisher Link]

[11] Zhe Jin, C.J. Kaalund, and Gangding Peng, "Novel Approach to Design High-Performance Large-Port-Count Switches in Low-Index-Contrast Materials Based on Cascaded Multimode Interference Couplers," *IEEE Journal of Quantum Electronics*, vol. 41, no. 12, pp. 1548-1551, 2005. [CrossRef] [Google Scholar] [Publisher Link]

[12] Meng Cui, and Changhuei Yang, "Implementation of a Digital Optical Phase Conjugation System and Its Application to Study the Robustness of Turbidity Suppression by Phase Conjugation," *Optics Express*, vol. 18, no. 4, pp. 3444-3455, 2010. [CrossRef] [Google Scholar] [Publisher Link]

[13] Zhiyang Li, "3D Display Based on Complete Digital Optical Phase Conjugation," *Optics Communications*, vol. 293, pp. 10-14, 2013. [CrossRef] [Google Scholar] [Publisher Link]

[14] Ioannis N. Papadopoulos et al., "Focusing and Scanning Light through a Multimode Optical Fiber Using Digital Phase Conjugation," *Optics Express*, vol. 20, no. 10, pp. 10583-10590, 2012. [CrossRef] [Google Scholar] [Publisher Link]

[15] Timothy R. Hillman et al., "Digital Optical Phase Conjugation for Delivering Two-Dimensional Images through Turbid Media," *Scientific Reports*, pp. 1-5, 2013. [CrossRef] [Google Scholar] [Publisher Link]

[16] Zhiyang Li, and Havyarimana Claver, "Compact Wavelength-Selective Optical Switch Based on Digital Optical Phase Conjugation," *Optics Express*, vol. 38, no. 22, pp. 4789-4792, 2013. [CrossRef] [Google Scholar] [Publisher Link]

[17] Havyarimana Claver, and Zhiyang Li, "Architecture to Integrate a Large-Scale DOPC-Based Optical Switching System on a Chip," *Journal of Optical Communications and Networking*, vol. 7, no. 7, pp. 602-608, 2015. [CrossRef] [Google Scholar] [Publisher Link]

[18] Yuhan Yao et al. "Performance of Integrated Optical Switches Based on 2D Materials and Beyond," *Frontiers of Optoelectronics*, vol. 13, pp. 129-138, 2020. [CrossRef] [Google Scholar] [Publisher Link]

[19] M.P. Earnshaw et al., "Compact, Low-Loss 4×4 Optical Switch Matrix Using Multimode Interferometers," *Electronics Letters*, vol. 37, no. 2, pp. 115-116, 2001. [CrossRef] [Google Scholar] [Publisher Link]

[20] E.J. Murphy et al., "16/spl Times/16 Strictly Nonblocking Guided-Wave Optical Switching System," *Journal of Lightwave Technology*, vol. 14, no. 3, pp. 352-358, 1996. [CrossRef] [Google Scholar] [Publisher Link]

[21] R.P. Schreieck et al., "All-Optical Switching at Multi-100-Gb/S Data Rates with Mach-Zehnder Interferometer Switches," *IEEE Journal of Quantum Electronics*, vol. 38, no. 8, pp. 1053-1061, 2002. [CrossRef] [Google Scholar] [Publisher Link]

[22] Abdulaziz Mohammed Al-Hetar et al., "MMI-MZI Polymer Thermo-Optic Switch with a High Refractive Index Contrast," *Journal of Lightwave Technology*, vol. 29, no. 2, pp. 171-178, 2011. [CrossRef] [Google Scholar] [Publisher Link]

[23] Hiroki Kishikawa et al., "All-Optical Wavelength-Selective Switch Consisting of Asymmetric X-Junction Couplers and Raman Amplifiers for Wide Wavelength Range," *Journal of Lightwave Technology*, vol. 28, no. 1, pp. 172-180, 2010. [Google Scholar] [Publisher Link]

[24] Muhammad A. Butt, Nikolay L. Kazanskiy, and Svetlana N. Khonina, "Advances in Waveguide Bragg Grating Structures, Platforms, and Applications: An Up-to-Date Appraisal," *Biosensors*, vol. 12, no. 7, pp. 1-28, 2022. [CrossRef] [Google Scholar] [Publisher Link]

[25] L.B. Soldano, and E.C.M. Pennings, "Optical Multi-Mode Interference Devices Based on Self-Imaging: Principles and Applications," *Journal of Lightwave Technology*, vol. 13, no. 4, pp. 615-627, 1995. [CrossRef] [Google Scholar] [Publisher Link]

[26] R. Ulrich, and J. Ankele, "Self-Imaging in Homogeneous Planar Optical Waveguides," *Applied Physics Letters*, vol. 27, no. 6, pp. 337-339, 1975. [CrossRef] [Google Scholar] [Publisher Link]

[27] M. Bachmann, P.A. Besse, and H. Melchior, "General Self-Imaging Properties in $N \times N$ Multimode Interference Couplers Including Phase Relations," *Applied Optics*, vol. 33, no. 18, pp. 3905-3911, 1994. [CrossRef] [Google Scholar] [Publisher Link]

[28] S.T. Chu, and S.K. Chaudhuri, "A Finite-Difference Time-Domain Method for the Design and Analysis of Guided-Wave Optical Structures," *Journal of Lightwave Technology*, vol. 7, no. 12, pp. 2033-2038, 1989. [CrossRef] [Google Scholar] [Publisher Link]

[29] John B. Schneider, *Understanding the Finite-Difference Time-Domain Method*, School of electrical engineering and computer science Washington State University, pp. 1-413, 2010. [Google Scholar] [Publisher Link]

[30] F.L. Teixeira et al., "Finite-Difference Time-Domain Methods," *Nature Reviews Methods Primers*, vol. 3, 2023. [CrossRef] [Google Scholar] [Publisher Link]